

Manuscript [hess-2020-188](#): “*Spatial distribution of tracers for optical sensing of stream surface flow*” by Pizarro et al.

We report a detailed response to each of the comments and suggestions below (text in red).

5

Reviewer 1

Obs. 1: This study reports a novel approach to refining image-based flow velocity estimates, with a specific focus on the effects of particle seeding. The use of simulated images to isolate these factors while eliminating the confounding effects of other environmental variables is innovative and could be a useful approach for conducting similar controlled experiments in the future. The paper is generally well-organized and reasonably well written, and the figures are clear and insightful, so I am generally supportive of the work and believe that the manuscript could be published pending some minor revisions. Please refer to the attached PDF for the details, as well as a large number of in-line text edits to improve English usage, but here are a few of the highlights:

15

Ans. 1: We thank the anonymous Reviewer 1 for the detailed feedback, comments, and suggestions provided.

Obs. 2: Title: I suggest augmenting the title a bit to make what you actually did in this study more clear, perhaps start with “Identifying the optimal density and ...”

20

Ans. 2: We agree with the reviewer and decided to change the title as follows: “*Identifying the optimal spatial distribution of tracers for optical sensing of stream surface flow*”.

Obs. 3: Line 11: You need to clarify from the beginning what you mean by aggregation. It wasn’t until well into the paper that I got a clear understanding of what you mean by this term. Essentially clustering or dispersion of the tracers, right?

25

Ans. 3: Thank you for pointing out this issue. In order to avoid confusion, we will only refer to the term clustering or dispersion rather than aggregation.

Obs. 4: Line 17: Similarly, clarify what you mean by converging seeding density - is this only in areas where the flow streamlines come together? I never really got a clear sense of what this refers to.

30

35 Ans. 4: We agree with the reviewer, and we thank him/her for pointing out this aspect. The term was improperly used to identify the minimum seeding density that assures an error of about 2 – 3% in Figure 4. This error value is a reference value after which an asymptotic behaviour of the errors is observed. We will reformulate the description on lines 217 – 220 to better clarify this concept.

Obs. 5: Line 58: This would be a good place to elaborate a bit on what you mean by this term (aggregation).

40 Ans. 5: See Ans. 3.

Obs. 6: Line 78: Relative in what sense? In comparison to field measurements? Please clarify.

Ans. 6: Thank you for this comment. The word “*relative*” will be removed in the new version of the manuscript.

45 Obs. 7: Line 88: This (unidirectional, constant velocity) is a significant and somewhat unrealistic assumption and I think you should acknowledge this in some way within the text.

Ans. 7: We appreciate this suggestion since it is an explicit limitation of the proposed framework. Therefore, we will add a final section introducing the strengths and limitations of this research.

50 Obs. 8: Line 134: What kind (of current meter)? Please provide more detail, similar to the level of detail used to describe the camera system.

55 Ans. 8: Velocities and river discharge were measured using a current meter (SEBA F1, SEBA Hydrometrie GmbH & Co, Kaufbeuren, Germany). The accuracy of measurements is within 2% of the measured values, corresponding to 0.001 and 0.014 m/s for the minimum and maximum velocities in question. This information will be added to the main text, respectively.

60 Obs. 9: Line 138: Were there two different kinds of tracers? The last couple of sentences of this paragraph are unclear.

Ans. 9: Only one type of artificial tracers (wood chip) was considered to extra seed the ROI. Two operators were involved in the process of deploying the material. The sentence in question will be slightly modified to be clearer.

65

Obs. 10: Line 156: This figure (3) appears to have only one image, not an original and enhanced version. Please modify the text and caption to remove the reference to the original image, or update the figure to include the raw image.

70 Ans. 10: Figure 3.B shows two images in one. Riverbanks are shown in the original greyscale acquisition modality, while the darker area where water flows corresponds to the same pre-processed frame overlapping this area. A better explanation of this figure will be added to the main text in the new version of the manuscript.

75 Obs. 11: Line 168: Did you try the new ensemble correlation method available within PIVlab? This approach is designed for low particle densities and could be helpful in this study, so I suggest adding a bit of analysis to assess the performance of the ensemble correlation method in addition to the standard PIVlab technique.

80 Ans. 11: Thank you for pointing out this matter. We did not apply the new-available-in-PIVLab ensemble correlation method within our analysis, mainly motivated by the small number of frames used within the synthetic framework (20 synthetic images). To have full benefits of the ensemble correlation method, it is suggested a large number of images and low seeding conditions. Nevertheless, this matter can be
85 considered for future research.

References:

1. <https://pivlab.blogspot.com/2019/09/the-benefit-of-ensemble-correlation-in.html>
- 90 2. Westerweel, J.; Geelhoed, P.F.; Lindken, R. Single-pixel resolution ensemble correlation for micro-PIV applications. *Exp Fluids* 2004, 37, 375–384.

Obs. 12: Line 170: Were the SA and IA the same? Typically, the step size is half the size of the IA.

95 Ans. 12: IA was the half of SA for the three passes considered within the analyses as is shown between parentheses on line 170 (e.g., 128x64). We will slightly modify the sentence to clarify this issue better.

100 Obs. 13: Figure 4: These graphs are a bit confusing at first glance because the error values are all negative, which makes the axes appear backward because smaller errors actually plot higher on the graph. You might want to point this out in the text to help the reader understand how to interpret these plots.

105 Ans. 13: Thank you for this suggestion. This matter is already explicitly written on lines 190 – 193 (before Figure 4), where it is pointed out that only negative errors were observed within numerical analyses. Nevertheless, a clarification will be added to the figure caption.

110 Obs. 14: Line 218: I still don't know what you mean by converging seeding density.

Ans. 14: Please, see Ans. 4.

115 Obs. 15: Line 270: You should provide some more information about this algorithm.

Ans. 15: Thank you for this suggestion. More information will be added to the main text to clarify better how the algorithms work. Further information about this algorithm is also provided in the following paper:

120 1. Dal Sasso, S.F.; Pizarro, A.; Manfreda, S., Metrics for the Quantification of Seeding Characteristics to Enhance Image Velocimetry Performance in Rivers. Remote Sens. 2020, 12, 1789.

Obs. 16: Please also note the supplement to this comment.

125 Ans. 16: We would like to thank again Reviewer 1 for the detailed feedback provided. We will go through the supplement document in detail, checking all the matters pointed out.

Reviewer 2

130 Obs. 1: The manuscript investigates on the seeding density role for image analysis algorithms (PTV and
LSPIV) useful for surface velocity measurements. Moreover, authors propose a dimensionless index for
evaluating performances of algorithms. The topic is surely interesting and the manuscript is well
organised and easy to follow. In the last twenty years the attempt to use camera for estimating river surface
velocity is becoming always more reliable and, in general, gauge-cams are promising instruments that
soon will be widely adopted. However, there are still several bottlenecks that should be, and will be, soon
135 solved either in the hardware and in the software behind this relatively new methodology. One of these,
is the absence of benchmarks for evaluating and comparing performances of image analysis algorithms
(PTV, LSPIV, OTV, etc.). This manuscript goes toward this direction providing a simple framework for
analysing the seeding density role. So, I positively evaluate the manuscript since, about this research topic,
is not easy, or better impossible, to have available reliable benchmark, so the idea of synthetic scenarios
140 is welcome. Following this general assessment, I have some further comments to share with the authors.

Ans. 1: We would like to thank the anonymous Reviewer 2 for the positive feedback, suggestions, and
further comments.

145 Obs. 2: Lines 30-35. I found reductive these lines for emphasising the usefulness of non-contact
approaches. Such approaches allow to measure surface velocities (and so indirectly discharge) during a
flood, that is not possible to observe with common methods. So, it represents really a crucial and
significant advancement of knowledge.

150 Ans. 2: Thank you for pointing out this matter. We agree with reviewer 2, and the sentence will be slightly
modified in the new version of this manuscript to highlight better the importance of using non-contact
approaches at high flow conditions.

Obs. 3: Lines 49-50. Maybe the difference between PTV and LSPIV could be better described referring
to the “eulerian” and “lagrangian” characterisation.

155 Ans. 3: The sentence will be modified to add this information to the main text.

Obs. 4: Line 51. Unfortunately, or fortunately, these are still not “widely” used.

160 Ans. 4: To the authors’ knowledge, several researchers, practitioners, and institutions are starting to use image-based techniques to observe/estimate surface flow velocities and river stream flows remotely. Among them, initiatives in Italy, France, Switzerland, the UK, Australia, Japan, Chile, Peru, Argentina, and the USA are examples of it (see some references below). Therefore, and despite their use worldwide, uncertainty within the measurements is still an open issue motivating not only the sentence in question but also the research the authors are carrying out.

165

References:

1. <https://flood-obs.com/>
2. <https://floodscale.irstea.fr/front-page-en>
- 170 3. https://twitter.com/CdC_Cordoba
4. https://www.usgs.gov/mission-areas/water-resources/science/usgs-next-generation-water-observing-system-ngwos?utm_source=twitter&utm_medium=social&utm_term=f0750e58-49ba-48cb-a985-46a71dc3f83c&utm_content=&utm_campaign=usgs&qt-science_center_objects=0#qt-science_center_objects
- 175 5. <https://discharge.ch/>

Obs. 5: Line 127. How discharge and velocities were estimated or measured?

180 Ans. 5: Velocities were measured using a current meter (SEBA F1, SEBA Hydrometrie GmbH & Co, Kaufbeuren, Germany). The accuracy of measurements is within 2% of the measured values, corresponding to 0.001 and 0.013 m/s for the minimum and maximum velocities in question. River discharge was estimated according to ISO-748/1997, using the velocity-area method. The cross-section was divided into panels of equal width and, for each panel, the velocity was measured at 20%, 60% and 80% of the panel depth.

185 Reference:

1. International Standards Organization (ISO). Measurement of Liquid Flow in Open Channel—Velocity-Area Method; ISO 748; ISO: Geneva, Switzerland, 1997.

190 Obs. 6: Figure 4. I am very glad to see the figure 4 that clearly shows how the PTV outperforms LSPIV. It is a pity that authors (line 185) did not apply any post-processing on the results. Comparing PTVLab and PTVLab+post processing, results are significantly different, indeed the potentiality of PTV is in the opportunity in validating trajectories avoiding fake information. In any case, it is already clear from the results that PIV suffers more than PTV of the seeding density. Maybe the final percentage errors would be different for the two methods. I would mention in the conclusion or in the discussion that the difference
195 between PTV and LSPIV is expected to be higher in case of using post processing analyses.

200 Ans. 6: We are aware of possible post-processing methodologies. However, from the authors' point of view, many of them are subjective and user-dependent despite their logical concept. Therefore, we decided to standardise the analysis giving the same conditions for both techniques, namely PTV and PIV. In addition, one of the main goals of this research was the discovery of seeding characteristics trends with the intention to minimise image-velocimetry errors. Post-processing methodologies would potentially hide them due to their filtering nature. Nevertheless, this matter is without a doubt, an issue to be considered for future research.

Editor

205 Obs. 1: Dear Authors, Your original submission just received some interesting comments from two reviewers. I invite you to provide some preliminary responses so as to suitably feed the discussion step of the journal and possibly receive further comments from these experts.

210 Ans. 1: We would like to thank the Editor for this suggestion that without a doubt will promote the discussion. We included our responses to the reviewers addressing their suggestions.

Reviewer 3

Obs. 1: This manuscript deals with the image velocimetry method and suggests a new metric to evaluate the seeding quality. The study is interesting, but there are some issues that need to be addressed.

215

Ans. 1: We thank the anonymous Reviewer 3 for the detailed feedback, comments, and suggestions provided.

Obs. 2: There are some vague sentences.

220

Ans. 2: We will revise the text carefully to avoid any vague sentence and lack of clarity.

Obs. 3: At some points, the text lacks the necessary details to fully comprehend the steps followed. For example, the authors do not provide any information on how the motion of the particles of the synthetic images was simulated. Similarly, the concept behind some assumptions is not explained (see below the comment about "multiplication of power laws" and the comment about $v=D$).

225

Ans. 3: Thank you for pointing out this matter. Please, see Ans 2, Ans. 16, and Ans. 18.

Obs. 4: The value of the suggested index is not fully demonstrated. The authors need to show what would be the error if all frames were used instead of selecting frames based on the suggested index.

230

Ans. 4: Please, see Ans. 21.

Obs. 5: The well known constant π is used as a symbol for the suggested metric. This is like using number 1 as a symbol for a variable or index.

Ans. 5: Please, see Ans. 6.

235 Obs. 6: The specific locations in the manuscript of the previous general comments are given below. Location: "A descriptor of the seeding characteristics (based on density and aggregation) was introduced based on a newly developed metric π ." Comment: In mathematics, the Greek letter π is reserved to be used for one and only one thing, the ratio of a circle's circumference to its diameter. Please use another symbol (e.g., "SCD")

240

Ans. 6: We appreciate the reviewer for bringing us this issue. The Greek letter " π " is frequently used to define dimensionless parameters. Nevertheless, and with the intention to avoid any confusion, a different symbol will be adopted in the revised version of the manuscript.

References:

245

1. Buckingham, E. (1914). On physically similar systems; illustrations of the use of dimensional equations. *Physical review*, 4(4), 345.

2. Evans, J. H. (1972). Dimensional analysis and the Buckingham pi theorem. *American Journal of Physics*, 40(12), 1815-1822.

250

3. Melville, B. W., & Sutherland, A. J. (1988). Design method for local scour at bridge piers. *Journal of Hydraulic Engineering*, 114(10), 1210-1226.

4. Hanche-Olsen, H. (2004). Buckingham's pi-theorem. NTNU: <http://www.math.ntnu.no/~hanche/notes/buckingham/buckingham-a4.pdf>.

255

5. Pizarro, A., Ettmer, B., Manfreda, S., Rojas, A., & Link, O. (2017). Dimensionless effective flow work for estimation of pier scour caused by flood waves. *Journal of Hydraulic Engineering*, 143(7), 06017006.

Obs. 7: Location: "A reduction of image-velocimetry errors was systematically observed by decreasing the values of π " Comment: Since this is a metric, not a parameter that can be directly adjusted, it would be better to write "A reduction of image-velocimetry errors was systematically observed with lower values of SCD"

260

Ans. 7: The sentence will be reformulated in the revised version of the manuscript to avoid any lack of clarity within the text.

Obs. 8: Location: Equation 1 Comment: It looks like S is missing after the exp(1).

Ans. 8: Thank you for pointing out this matter. Indeed, there is a typing error that will be amended in the revised version of the manuscript.

265

Obs. 9: Location: "The range of variability was established based on the ..." Comment: Does this refer to the values of the previous sentence?

Ans. 9: The sentence in question refers to the values written in the previous sentence, i.e. "*14 different seeding densities ranging from 0.4E-05 particles per pixel (ppp) up to 1.0E-02 (ppp)*".

270

Obs. 10: Location: "Furthermore, each numerical experiment contains 20 images, ..." Comment: How these 20 images were created?

Ans. 10: Synthetic images were generated using a Matlab code written by the authors for this purpose. The spatial distribution of synthetic tracers follows the Generalised Poisson Distribution (GPD),

275

280 presented in Eq. (1) of the manuscript. The main advantage of using this numerical approach is the fact that the seeding density and the clustering level of synthetic tracers can be controlled and associated to a parameter (ν and λ) of the GPD. Synthetic tracers move with a constant velocity of 15 pixels/frame along the y-axis. A numerical experiment was defined as 20 synthetic generated images following the mentioned information. All the data used in this study is freely available at <https://doi.org/10.5281/zenodo.3761859>.

Obs. 11: Location: "δ IIR ranges from 0.5 to 200 (12 different values) ..." Comment: It is very unusual to start a sentence with a lowercase variable.

285 Ans. 11: The sentence will be rephrased.

Obs. 12: Location: Lines 163-175 Comment: These lines should be broken into two paragraphs, one for PTV and one for PIV.

290 Ans. 12: The new version of the manuscript will take this issue into consideration.

Obs. 13: Location: "The theoretical velocity was set at 15 px/frame ..." Comment: This term("theoretical velocity") is repeated many times in the manuscript, but its meaning has not been defined

295 Ans. 13: Thank you for pointing out this matter. The "*theoretical velocity*" term will be defined at line 99, within the Numerical Simulation Section.

Obs. 14: Location: "... used 8 and 20 (px) " Comment: The unit px appears both inside parenthesis and without parenthesis (preferable) in the text.

300 Ans. 14: We will standardise the text in the revised version of the manuscript to avoid lack of consistency or clarity.

Obs. 15: Location: "PTV used 8 and 20 (px) for detection and tracking, respectively. PIV used FFT with three-passes (128x64, 64x32, 32x16)." Comment: This information has been already given (and more clearly) previously. It would be better to remove these sentences.

305 Ans. 15: This repeated information will be removed from the main text in the revised version of the manuscript.

Obs. 16: Location: "where f = function" Comment: This is not a solid definition, neither from a linguistic nor from a mathematical point of view. c Location: "The function f is usually considered as a multiplication of power laws." Comment: A reference is required.

310 Ans. 16: Thank you for bringing us this issue. The sentence in question will be reformulated to avoid confusion. Furthermore, the references given in Ans. 6 will be added at this point.

Obs. 17: Location: " ρ_{hov1} values for PIV and PTV were taken from Figure 4 and are 1.52E-03 and 1.02E-03," Comment: The error, for low error values, is not very sensitive on the suggested metric. What if a single ' $v=1$ converging seeding density' was used for both PTV and PIV? This would reduce the number of parameters.

320 Ans. 17: Although PIV and PTV are useful for image-based velocity estimates, they rely on different algorithms. In consequence, it is conceptually reasonable that the minimum seeding density assuring an error of about 2 – 3% in Figure 4 were different. Furthermore, the number of parameters will not be reduced since it does not modify π or Eq. (5).

Obs. 18: Location: "the empirical aggregation level (i.e., the empirical one equivalent to the used in the numerical simulations), was quantified through the dispersion index D ." Comment: This approach, which assumes D as an estimator of v , needs to be justified and explained with more details.

325 Ans. 18: Thank you for pointing out this issue. We agree with the reviewer that more details should be given at this regard. The new version of the manuscript will cover this issue as well as the introduction of a new section called "*Strengths and Limitations*" of this research.

330 Obs. 19: Location: "A moving window of 100 frames was arbitrarily chosen," Comment: What exactly was chosen arbitrarily, the length of the window?

Ans. 19: The length of the window was arbitrarily chosen, corresponding with 100 frames. The sentence will be reformulated to avoid confusion.

335 Obs. 20: Location: "Figure 8.A shows the particular case of PTV; nevertheless, PIV presented similar results. The locations of the minimum and maximum π values was, therefore, unaffected by the image-velocimetry technique under consideration." Comment: Why PTV and PIV would present different values for the suggested index? Is it because of the different ρ_{hov1} used for each method? If so, then this (the fact that PIV and PTV presented similar results) is an indication of using a single ρ_{hov1} value for both methods (see previous comment)

340 Ans. 20: Thank you for this observation. Please, see Ans. 18 as well. Indeed, PTV and PIV presented
different π values because of ρ_{cv1} . However, using the same ρ_{cv1} for both PIV and PTV is equivalent to
assume that both algorithms work in the same way (which is far from being right). Additionally, ρ_{cv1} was
estimated using a huge numerical framework, resulting in different values for PIV and PTV. Finally, there
is no advantage in using only one common value since the number of coefficients remains invariable.

345

Obs. 21: Location: Table 2 Comment: What would be the error if all frames were used?

Ans. 21: The average absolute errors calculated using PTV and PIV if all frames were used are 23.93%
and 23.69%, respectively. Nevertheless, this research introduced a new dimensionless parameter able to
identify the best location of N frames, minimising image-based errors. Comparing these errors with the
ones using π , it is possible to appreciate that they are essentially the same (23.31% and 24.11% for PTV
and PIV, respectively); even though the number of frames used with π is the half with respect to the total
number of frames. A sentence will be added to the “*Strengths and Limitations*” section, highlighting this
matter. Finally, the authors are currently working with a larger dataset to generalise the methodology.

355

Identifying the optimal Spatial distribution of tracers for optical sensing of stream surface flow

Alonso Pizarro¹, Silvano F. Dal Sasso¹, Matthew T. Perks², Salvatore Manfreda³

¹Department of European and Mediterranean Cultures, University of Basilicata, Matera, 75100, Italy

360 ²School of Geography, Politics and Sociology, Newcastle University, Newcastle-upon-Tyne, NE1 7RU, UK

³Department of Civil, Architectural and Environmental Engineering, University of Naples Federico II, Naples, 80125, Italy

Correspondence to: Alonso Pizarro (alonso.pizarro@unibas.it)

Abstract. River monitoring is of particular interest for our society that is facing increasing complexity in water management. Emerging technologies have contributed to opening new avenues for improving our monitoring capabilities, but also generating new challenges for the harmonised use of devices and algorithms. In this context, optical sensing techniques for stream surface flow velocities are strongly influenced by tracer characteristics such as seeding density and their spatial clustering distribution level of aggregation tracers. Therefore, a principal research goal requirement is the identification of how these properties affect the accuracy of such methods. To this aim, numerical simulations were performed to consider different levels of particle aggregation tracer clustering, particle colour (in terms of greyscale intensity), seeding density, and background noise. Two widely used image-velocimetry algorithms were adopted: i) Particle Tracking Velocimetry (PTV), and ii) Large-Scale Particle Image Velocimetry (LSPIV). A descriptor of the seeding characteristics (based on seeding density and their aggregation spatial tracer clustering) was introduced based on a newly developed metric called Seeding Distribution Index (SDI) $\#$. This value-index can be approximated and used in practice as $\#SDI = v^{0.1} / \left(\frac{\rho}{\rho_{cv1}} \right)$ where v , ρ , and ρ_{cv1} are the aggregation spatial clustering level, the seeding density, and the converging-reference seeding density at $v = 1$, respectively. A reduction of image-velocimetry errors was systematically observed by decreasing the with for lower values of SDI $\#$; and therefore, the optimal frame window (i.e., a subset of the video image sequence) was defined as the one that minimises SDI $\#$. In addition to numerical analyses, the Basento field case study on the Basento river (located in southern Italy) was considered as a proof-of-concept of the proposed framework. Field results corroborated numerical findings, and an error reductions of about 15.9 and 16.1% was-were calculated - using PTV and PIV, respectively - by employing the optimal frame window.

380 1 Introduction

SRiver streamflow observations are of enormous importance for environmental protection and engineering practice in general (Anderson et al., 2006; Manfreda, 2018; Manfreda et al., 2020; Owe, 1985). Such observations are critical for many hydrological and hydraulic applications. In turn, it enables the understanding of more complex processes such as flash flood dynamics (Perks et al., 2016), the interaction of fish upstream and downstream of dams (Strelnikova et al., 2020), sediment transport dynamics (Batalla and Vericat, 2009), and bridge scour (Manfreda et al., 2018a; Pizarro et al., 2017a).

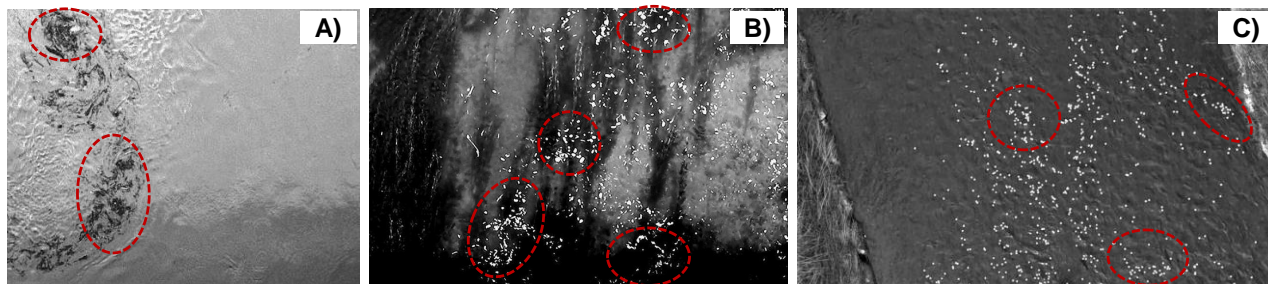
385

Streamflow measurement campaigns are generally expensive and time-consuming, requiring the presence of highly-qualified personnel and forward planning (Tauro et al., 2018). Such approaches are typically based on pointwise measurements performed with flowmeters or acoustic ~~deoppler-Doppler~~ current profilers (ADCPs) that require the direct ~~access-placement~~ of the operators or devices into the water. On the one hand, this is necessary to provide a full description of the flow velocity profile, but on the other hand, it may alter the measurements given the potential interaction of these elements with the ~~flux-flow~~. Additionally, these is standard approaches can be challenging and sometimes impossible to perform at flood conditions when operators and devices are unable to work in-situ due to in-situ hazardunfavourable circumstances. This issue has been partially dealt with by the use of non-contact approaches, as a ~~timely-modern~~ alternative for river flow monitoring. Progress in the development of non-contact approaches (such as image velocimetry, radars, and microwave systems) has been promising in recent years, opening the possibility for real-time, non-contact, flow monitoring. In particular, ~~the~~ ~~advancements~~ ~~of-in~~ image processing techniques have led to improvements of image-based approaches for surface flow velocity (SFV) estimation, and ~~these~~ ~~developments~~ ~~havehas~~ ~~enhanced-expanded~~ the range of potential applications. Several techniques, such as Particle Tracking Velocimetry (PTV) and Large-Scale Image Velocimetry (LSPIV), have been proposed and applied in field campaigns to accurately estimate SFV from video acquisitions (Bechle et al., 2012; Huang et al., 2018; Tauro and Salvatori, 2017). In turn, videos can be recorded from different devices (fixed-station located close to the river-section of interest, using cell phones, or onboard Unmanned Aerial Systems (UASs)), allowing an easy and portable way to estimate SFVs and, consequently, river discharge (Leitão et al., 2018; Manfreda et al., 2018b; Pearce et al., 2020; Perks et al., 2016; Tauro et al., 2015).

The PTV technique revolves around particle identification and tracking (Lloyd et al., 1995) that can be implemented through cross-correlation (Brevis et al., 2011; Lloyd et al., 1995), relaxation (Wu and Pairman, 1995), among other methods. Additionally, particle trajectories can be reconstructed, adding valuable information to the analysis and making it possible to apply trajectory-based filters to ensure realistic trajectories (Eltner et al., 2020; Tauro et al., 2019). On the other side, LSPIV techniques apply Particle Image Velocimetry (PIV) principles (Adrian, 1991, 2005; Peterson et al., 2008; Raffel et al., 2018) to large scales and natural environments (Fujita et al., 1998). ~~Interesting to mention,~~ LSPIV recognises and tracks patterns (which can be a group of tracers within a discrete spatial portion of the water surface) instead of single tracers, ~~while-which~~ are tracked in PTV-single tracers. As a consequence, PTV adopts an exclusively Lagrangian approach, while PIV an Eulerian one.

~~The use of t~~These techniques ~~are-is~~ widely-usedgrowing in recent years, but it is hard to quantify their accuracy at field scales. This difficulty can be ~~influenced-by~~ attributed to: i) environmental conditions, which can both deteriorate and enhance the image quality during the acquisition period (Le Coz et al., 2010; Muste et al., 2008); and ii) the characteristics of the tracers/features, such as colour, dimension, shape, seeding density, and their spatial clustering-aggregation leveldistribution in the field of view (Dal Sasso et al., 2018, 2020; Raffel et al., 2018). PTV and LSPIV need features to identify, match, and track to compute surface flow velocities. High seeding densities are, however, rare in natural environments and, as a consequence, a general-common practice is the use of artificial tracers to increase the surface seeding in the field of view (Dal Sasso et al., 2018; Tauro et al., 2014, 2017). In this context, Figure 1 shows three different real case-study examples of natural and artificial

420 seedings that tend to cluster. Remarkably, Figure 1.A reports high ~~seeding-spatial aggregation-clustering~~ levels ~~of tracers~~ and complex ~~cluster~~-structures during a flood event at the Tiber river in Italy (Tauro et al., 2017), whereas Figure 1.B and 1.C present the case when artificial seeding is introduced in the river system for image-velocimetry analysis (Detert et al., 2017; Tauro et al., 2017). More information about the mentioned case studies can be found elsewhere (Perks et al., 2019).



425 **Figure 1. Examples of moving and ~~aggregated-clustering~~ structures on the water surface: A) Natural seeding during a flood event at the Tiber river, Italy (Tauro et al., 2017); B) and C) Artificial seeding at low/intermediate flow conditions at Brenta river in Italy (Tauro et al., 2017) and Murg river in Switzerland (Detert et al., 2017), respectively.**

The spatial distribution of artificial tracers (~~hereafter called spatial clustering~~) is, however, operator-dependent and influenced by their experience, the type of material deployed, and amount. External environmental and river conditions such as wind and turbulence are also important factors. This issue is extremely relevant for discharge estimates recovered through image-based approaches ~~because since~~-velocity errors are transmitted to streamflow estimations. ~~In-As a~~ consequence, and even ~~by-when~~ using up-to-date approaches, monitoring complex flows, and extreme flood events, ~~is~~ still a challenge.

This paper aims to quantify the accuracy of SFV estimates under different seeding densities and ~~aggregation-spatial clustering~~ levels. To achieve this ~~goal~~, the following objectives were proposed: i) ~~generation-of-perform~~ numerical simulations of synthetically ~~aggregated~~-tracers to produce 33,600 synthetic images ~~of-with~~ known seeding characteristics; ii) using these synthetic images, ~~derive~~ a functional relationship between seeding densities, ~~aggregations-spatial clustering~~ levels, and image velocimetry errors ~~was-derived~~ under controlled conditions; iii) ~~analysis-was-undertaken-analyse~~ on-footage acquired ~~of-from~~ the Basento River to determine how variations in seeding characteristics such as seeding density and ~~aggregation-spatial clustering of tracers level~~ influence the image velocimetry errors in an ~~uncontrolled~~ field environment. Finally, iv) ~~apply~~ the function developed in ii) ~~was-applied~~ to the Basento River to enable the selection of the optimal image frame sequence to minimise ~~the velocity relative~~-errors.

The rest of the paper is organised as follows: Section 2 presents the numerical framework for synthetic image generation; a description of the hydrological characteristics of the Basento case study, which is used as a proof-of-concept; and, an outline of the PTV and PIV techniques adopted in ~~the~~ analysis. Section 3 analyses the effects of seeding density and ~~aggregation~~ ~~spatial clustering~~ level on image-velocimetry results, using the synthetically generated images, and those of the Basento field case study. ~~Section 4 presents the strengths and limitations of the research and framework adopted in this paper.~~ Conclusions ~~at the end~~ are provided in Section 5.

2 Methods

2.1 Numerical Simulations

450 Numerical simulations were performed to test two different image-velocimetry algorithms under controlled conditions, minimising the effects of external disturbances. In particular, the influence of tracer/feature properties on the final errors were quantified. Synthetic tracers were randomly distributed in space with a unidirectional and constant velocity. They consist of uniform circular shapes with diameter $D_{xp} \approx 10$ pixels (px) and uniform white colour. Both diameters and colours ~~- in grayscale~~ intensity - were altered with white noise in order to consider more realistic configurations. Their spatial distribution was
455 controlled by a Generalised Poisson Distribution (GPD) with an imposed numerical ~~theoretical~~ seeding density λ and spatial clustering level ~~of aggregation~~ spatial clustering v .

The GPD was first introduced by Efron (1986), allowing the possibility to obtain point events randomly distributed in space with a given variance. The GPD has been used to model randomly distributed events in different studies to describe the spatial characteristics of the landscape and vegetation organisation across climatological gradients (~~for instance, e.g. Good, Rodriguez-~~
460 ~~Iturbe, and Caylor (2013) and Manfreda, Caylor, and Good (2017)~~ used the GPD to describe the spatial characteristics of the landscape and vegetation organisation across climatological gradients). In this manuscript, the synthetic tracers are assumed to be randomly distributed in space with a mean number λS where S is the considered area. In consequence, the probability mass function that the random number of synthetic tracers, N , will be equal to a number n_i is given by Eq. (1),

$$f_{GPD(\lambda S)}(n_i) = \frac{1}{C_{GPD}} \frac{\exp\left(-\frac{\lambda S}{v}\right)}{\sqrt{v}} \left(\frac{\exp(-n_i) n_i^{n_i}}{n_i!}\right) \left(\frac{\exp(1) \lambda S}{n_i}\right)^{n_i/v}, \quad (1)$$

where λS and v determine the location and the shape of $f_{GPD(\lambda S)}(n_i)$, and C_{GPD} is an integration constant.

465 Tracers moved with a constant numerically imposed velocity of 15 ~~(px/frame)~~ along the y-axis and within a grid of 500x500 pixels on a clear water -background as representative of ~~actual-real~~ environmental conditions. Tracer diameter was set larger than 2.5 pixels in order to avoid peak locking effects (Cardwell et al., 2011; Dal Sasso et al., 2018; Nobach et al., 2005). Typical tracer dimensions at laboratory and field scales motivated the choice of $D_{xp} \approx 10$ ~~(px)~~ for image-velocimetry experiments (Tauro et al., 2016).

470 Synthetic image sequences were generated by varying the number of tracers in the spatial domain, allowing the consideration of 14 different seeding densities ranging from 0.4E-05 particles per pixel (ppp) up to 1.0E-02 ~~(ppp)~~. These range of variability was established based on the typical values adopted in field surveys (Tauro and Grimaldi, 2017) and numerical studies (Dal Sasso et al., 2018). Tracer colour (in terms of greyscale intensity) and diameter were altered (by introducing ~~a~~ Gaussian white noises s with standard deviations s equal to 0.05 and 0.3, respectively) to simulate environmental signal noises ~~(such as possible~~
475 ~~changes in luminosity, brightness, and shadows)~~. Figure 2 shows an example of synthetic image generations with different spatial clustering levels ~~of aggregation~~ and a fixed value of seeding density. In particular, the spatial distribution of tracers moves from an over-dispersed organisation ($v = 0.5$), through a Poisson random distribution ($v = 1$) and an under-dispersed

one ($\nu = 100$), to a super under-dispersed distribution ($\nu = 200$). Figure 2 (A, B, C and D) presents the original synthetic generation on the clear water background, while Figure 2 (E, F, G and H) shows the pre-processed images, enhancing the contrast between tracers and background (See Section 2.3). Furthermore, each numerical experiment ~~contains~~ involved generating 20 images, and each configuration was run 10 times. The spatial clustering level ν -ranges from 0.5 to 200 (12 different values), and in consequence, 33,600 synthetic images were generated (14 different λ , 12 different ν , 20 images per configuration, and 10 times each configuration).

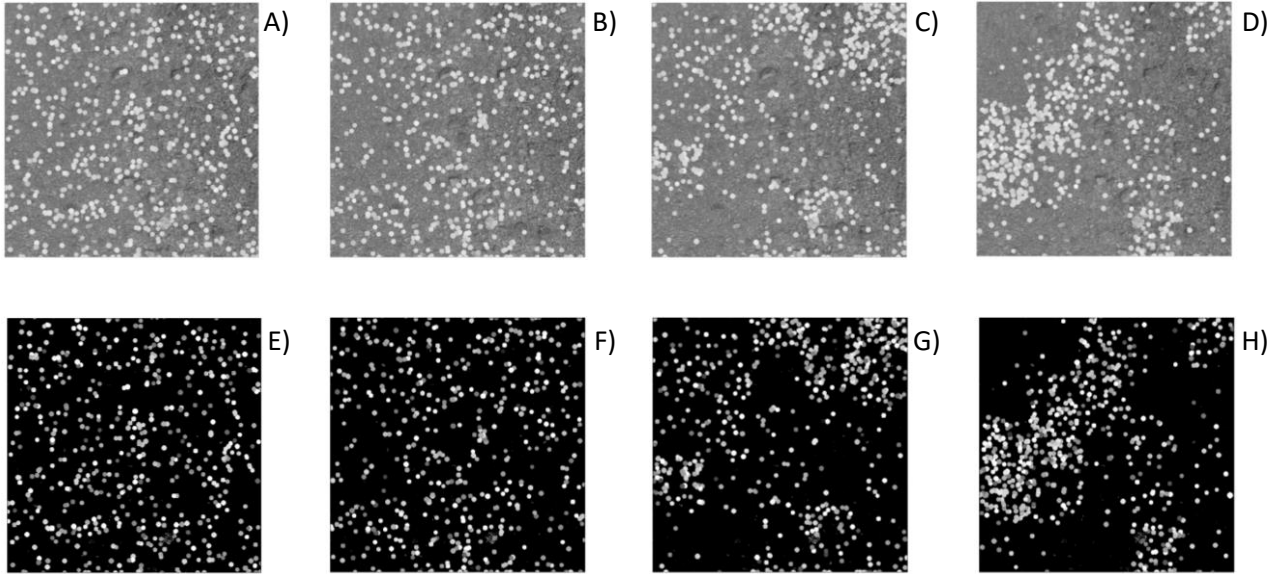


Figure 2. Synthetic generations of spatial distribution of tracers assuming different values of the aggregation-parameter $\nu = 0.5$ (over-dispersed distribution - Fig 2.A, E), 1.0 (Poisson random distribution - Fig 2.B, F), 100 (under-dispersed distribution - Fig 2.C, G), and 200 (super under-dispersed distribution - Fig 2.D, H). Fixed value of the seeding density $\lambda = 2.02E-03$. The generation was carried out adopting a background in the images to provide more realistic conditions (A, B, C, D). Thereafter, images have been pre-processed to increase the contrast and better visualise tracers (E, F, G, H).

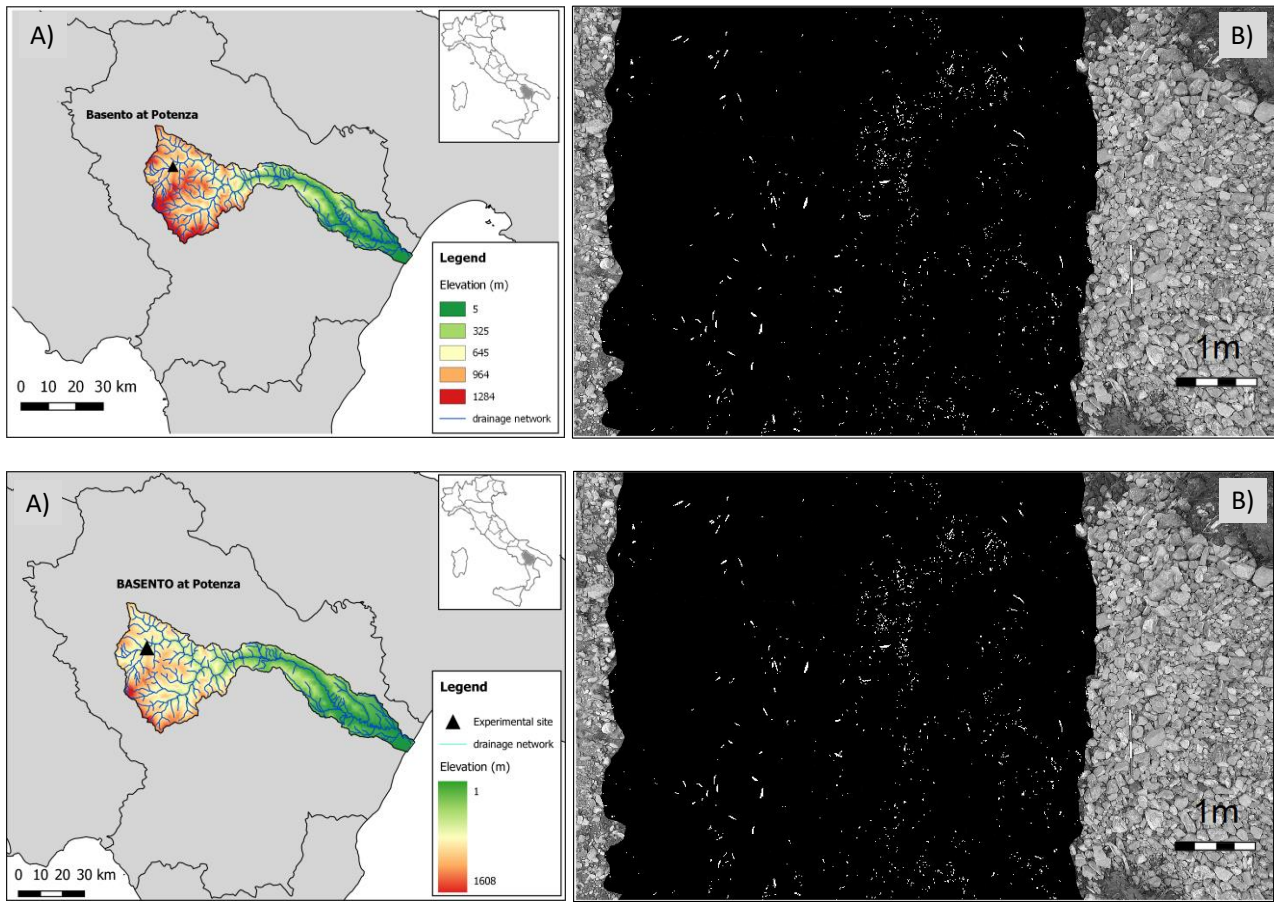
2.2 Proof-of-concept: The Basento case study

A field survey on the Basento River (Basilicata region, southern Italy) was carried out to test the outcomes of numerical simulations under real natural conditions. The cross-section considered for the measurements is located in the upper portion of the basin (catchment area of about 127 km²) (Figure 3). The main river flow characteristics, at the moment-time of the video acquisition, were: i) river streamflowdischarge: 0.61 (m³/s); ii) maximum flow depth: 0.38 (m); iii) river width: 6.0 (m); iv) maximum surface flow velocity: 0.68 (m/s); and, v) average surface flow velocity: 0.40 (m/s). Data were acquired using a DJI Phantom 3 Professional Quadcopter (DJI, Shenzhen, China) equipped with an integrated 4k UHD (ultra-high-definition) video recording camera and a 3-axis stabilised system. Video acquisition was performed using a Sony EXMOR 1/2.3" CMOS sensor and a greyscale video was captured from the UAS platform with a resolution of 1920x1080 (px) (i.e., Full High Definition - FHD). The ~~considered~~ frame rate was set to 24 frames per second (fps). Reference objects, useful for image scale calibration and stabilisation, were positioned at visible locations on the riverbanks. The calibration factor converting pixels to meters was

505 estimated, taking into consideration those objects with ~~a~~ known-a-priori dimensions. The ground sampling distance (GSD) was, therefore, computed as 0.005 (m/px). Benchmark velocity measurements were performed using a current meter (SEBA FI, SEBA Hydrometrie GmbH & Co, Kaufbeuren, Germany), in the proximity of the water-free surface, at 11 different locations across the river cross-section. The accuracy of measurements was within 2% of the measured values, corresponding to 0.001 and 0.013 m/s for the minimum and maximum velocities in question. The spanning distance between the respective measurements was 0.5 (m). Each measurement was made over a fixed acquisition period of 30 seconds. River discharge was estimated according to ISO -748 (1997), using the velocity-area method. The cross-section was divided into panels of equal width and, for each panel, the velocity was measured at 20%, 60% and 80% of the panel depth. Artificial seeding was ~~properly~~ deployed onto the water surface, giving the possibility to create complex aggregated-floating structures. Two operators were 510 involved in the process, and artificial tracers made of wood chips ~~only~~ were used to enhance particle seeding ~~extra-seed~~ the region of interest (ROI).

The videos captured with the UAS were first stabilised using an automatic feature selection method that identifies features in frame pairs, matching them to compute possible values of translation and rotation. The Features from Accelerated Segment Test (FAST) detection algorithm was applied to identify features on an ad-hoc ROI. To improve the feature matching accuracy, 515 at each step, the method utilises the Random Sample Consensus (RANSAC) filter ~~for~~ to remove unacceptable correspondences. The application of the stabilisation algorithm ~~has~~ allowed the effects of camera movements to be reduced throughout the duration of the video. Planimetric-Planar errors considering differences in translation and rotation were computed taking the first frame as the reference target. On average, the reduction due to the stabilisation process goes from 64 to 7 (px) for the ~~considered-Basento~~ case study. Therefore, movement in the original video is reduced by around 89%. The stabilisation 520 algorithm does not require Ground Control Points (GCPs) to be applied. Rather, it performs the detection of features automatically, ~~and-making~~ the stabilisation process ~~is, therefore,~~ a good alternative for non-experienced users.

The Basento River presented low-flow conditions leading us to subsample~~ing~~ the original video from 24 to 12 (fps). The choice of the appropriate frame rate was made to ensure, on the one hand, a frame-by-frame displacement bigger than particle dimension and, on the other hand, to minimise the effects of camera movement between frame pairs on the calculation of 525 surface velocity. ~~As already mentioned,~~ ~~t~~ The footage was acquired in greyscale ~~and-~~ ~~A~~ a pre-processing procedure was applied using ~~the~~ contrast stretching techniques to enhance the visibility of the artificial tracers against the background. For this purpose, GIMP (the GNU Image Manipulation Program) was utilised to adjust brightness and contrast. This procedure eliminated a large amount of noise caused by external reflections, improving the number of tracers identified and thus cross-correlation in the ROI. Figure 3.B shows a ~~composite~~ example of the original frames (river banks in grayscale), overlain by 530 ~~and-the~~ pre-processed image covering the extent of the active channel using GIMP (darker area overlapping the original frame).



535 **Figure 3. A) Basento river and its drainage basin with an indication of the measurement location (Basento at Potenza). B) Grayscale**
footage acquired with a DJI Phantom 3 Pro (river banks) and corresponding footage after the pre-processing (river flow) aimed at
enhancing contrast for particle identification.

2.3 Image velocimetry analysis

PTV analyses were carried out employing a command-line version of PTVLab software (Brevis et al., 2011) that have been automated in order to handle the number of synthetic images. Tracer detection was performed using the particle Gaussian mask correlation method (Ohmi and Li, 2000). Setting parameters in terms of particle diameter and reflectance intensity were set equal to 8 px and 70, respectively. Particle tracking was implemented using a cross-correlation algorithm (Wu and Pairman, 1995). The interrogation area (IA) was set at 20 px, cross-correlation threshold at 0.7, and neighbour similarity percentage at 25%. PTV parameter settings were slightly modified under field conditions due to the differences between the numerical and field datasets. In particular, the average tracer dimension in the field conditions was estimated as 5 px and therefore, the particle diameter was set equal to 4 px and the IA at 25 px.

540
545

PIV analyses were performed employing a command-line version of PIVLab software (Thielicke and Stamhuis, 2014) ~~written by the authors for the same purpose~~. The PIV algorithm was applied using the Fast Fourier Transform (FFT) with a three-passes standard correlation method. ~~For both numerical and field analysis, (search area (SA) and the interrogation area (IA) sizes were set for three passes of 128x64, 64x32, 32x16 px with 50% overlap)~~. Additionally, the 2x3-point Gaussian fit was employed to estimate the sub-pixel displacement peak. These ~~setting~~ parameters were carefully chosen to ~~assure-ensure~~ the right identification and tracking of synthetic tracers. ~~For instance, PTV used a particle diameter of 8 px, while the synthetic diameter had an average value of 10 px with a standard deviation of 0.3 px. In addition, tracer movements must be inside the IA (PTV) and SA (PIV) for their right correct identification. The imposed numerical theoretical velocity was set at 15 px/frame, while IA and SA were 20 and 32 px for PTV and PIV (minimum one of the three passes), respectively.~~

~~PTV parameter settings were slightly modified under field conditions due to the differences between the numerical and field datasets. In particular, the average tracer dimension at field conditions was estimated as 5 px and therefore, the particle diameter was set equal to 4 and the IA at 25 (px).~~

Finally, the quality of the results was determined by examining the magnitude of the errors that were computed as:

$$\epsilon = 100 \times \frac{(u_c - u_R)}{u_R}, \quad (2)$$

where u_c is the computed velocity and u_R is the ~~theoretical-numerically imposed~~ (numerical case taken as reference) or measured (field case) velocity.

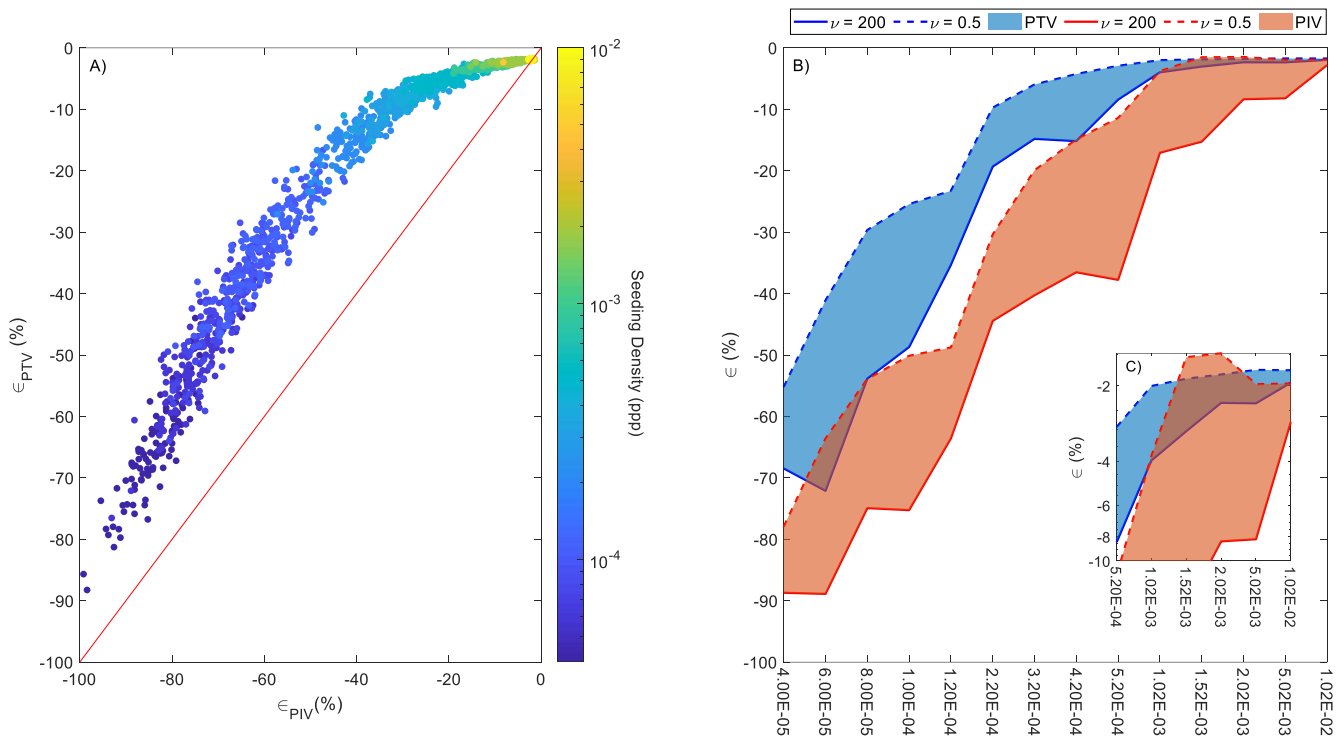
3 Results and Discussion

3.1 Numerical Analysis

The performance of PTV and PIV tracking algorithms was assessed by the calculation of errors (considering the imposed ~~theoretical-numerical~~ surface velocity) to test how the seeding density and ~~aggregation-spatial clustering level~~ distribution of tracers influenced ~~on~~ the final velocity estimates results. ~~PTV used 8 and 20 (px) for detection and tracking, respectively. PIV used FFT with three passes (128x64, 64x32, 32x16).~~ No post-processing method was applied to filter the spatiotemporal velocity results. The ROI was taken as the original dimension of the synthetic image generation, i.e. 500x500 (px). The processing times, considering ~~the 33,600~~ all the synthetically generated images, for ~~PIV and PTV and PIV~~ analyses were ~~4,736~~ 18,548 and ~~18,548-4,736~~ seconds, respectively. The same hardware (Processor i7-8700 CPU @ 3.20 GHz 3.19 GHz and RAM 32 GB) was used for both image-velocimetry analyses, leading to a fair comparison between them. PTV computing time was almost four times higher than PIV under the circumstances considered in this study. For all ~~the~~ cases, PTV and PIV techniques systematically underestimated the ~~theoretical-imposed numerical~~ velocity independently of the seeding density and ~~aggregation-spatial clustering~~ level under consideration. Consequently, only negative errors were observed with numerical results, in

575 agreement with previously published work (Dal Sasso et al., 2018). [This can be due to the use of a static background that may introduce sporadic zero velocity vectors.](#)

Figure 4 shows the PTV and PIV error results with different values of seeding densities and [aggregation-spatial clustering](#) levels. A comparison between PTV and PIV is shown in Figure 4.A, where each data point is associated with a colour that is scaled based on the [numerically theoretical-imposed numerical](#) seeding density adopted in the generation of synthetic images. A strong dependence between image-velocimetry results and seeding density was observed: errors can be reduced by increasing the seeding density. In all cases, PTV outperformed PIV under the synthetic conditions analysed in this study. These findings also support those of Tauro, Piscopia, and Grimaldi (2017) who found that PTV outperformed PIV in two different field case studies (Brenta and Tiber Rivers). It is [however](#) noteworthy that the [obtained](#) results [we present here](#) refer to a single synthetic experiment that, although realistic, is not representative of any field condition. Therefore, further investigations with a larger set of idealised and field circumstances should be carried out to generalise the obtained results.



590 **Figure 4. Comparison of PTV and PIV results using synthetic images with different values of seeding density and [aggregation-spatial clustering](#) level. [Only negative errors were observed with numerical results.](#) A) PTV vs PIV errors (ϵ_{PTV} and ϵ_{PIV} , respectively). Each data point is associated with a colour that is scaled based on the [numerically theoretical-imposed numerical](#) seeding density adopted in the numerical generation of synthetic images. B) Envelope error curves and areas in function of seeding density and level of [aggregation-spatial clustering](#) ν . The blue and orange colours are associated with PTV and PIV results, respectively. Dashed and solid lines are associated with $\nu = 0.5$ and $\nu = 200$, respectively. C) Zoom of the right upper portion of B).**

Figure 4.B shows the envelope error curves (and areas between them) for a range of seeding densities and level of [aggregation-spatial clustering](#) ν . The blue and orange colours are associated with PTV and PIV error results, while dashed and solid lines

595 are associated with $\nu = 0.5$ and $\nu = 200$, respectively. For the sake of simplicity, Figure 4.B only shows the extreme cases when
 $\nu = 0.5$ and $\nu = 200$; nevertheless, all the other cases (with ν values between these ~~two extremes~~~~considered cases~~) were confined
~~and~~ within these envelope curves. Error results of both techniques were influenced by ν , with a higher ~~aggregation-spatial~~
~~clustering~~ level tending to deteriorate the accuracy of image-velocimetry results, producing higher errors and associated
variability across the range of seeding densities. When the sensitivity of PIV and PTV to changes in ν are compared, ~~it is clear~~
600 ~~that~~ PIV is generally more sensitive than PTV, as demonstrated by the greater distance between $\nu = 0.5$ and $\nu = 200$ lines for
a given seeding density, and by the orange shaded area being greater than the blue. The minimum seeding density leading to
the ~~minimum-converging~~~~lowest~~ errors (around 2 – 3%) depended on ν . These errors were taken as reference values after which
an asymptotic behaviour was observed. As a consequence, this minimum seeding density concept was termed reference seeding
density in the rest of the paper. -For instance, considering the PIV case, the ~~converging-reference~~ seeding density values were
605 1.52E-03 and 1.02E-02 for $\nu = 0.5$ and $\nu = 200$, respectively. The ~~converging-reference~~ seeding density values for PTV were
1.02E-03 and 2.02E-03 for $\nu = 0.5$ and $\nu = 200$, respectively.

These numerical results are useful to visualise more-in-depth trends under controlled flow conditions, avoiding external
disturbances. Results demonstrated that the minimum required seeding density to produce an error equal or lower than 3%
differs slightly between the two techniques. We used this percentage as a reference error in order to derive a reference seeding
610 density associated with a known error. It was observed that PIV required 1.52E-03 (~~ppp~~), while PTV needed about 1.02E-03
(~~ppp~~) to reach the same error. Notably, seeding densities lower than 1.0E-03 produced larger errors (larger than 3%) and
consequently, flows should be ~~extra~~-seeded at least this density in field campaigns for optimal implementation of the methods.
This practice should always be adopted since typical natural flows are not characterised ~~for presenting elevated~~~~by abundant~~
transiting features, with maybe the exception of high flows. Furthermore, the effective seeding density (defined as the seeding
615 that the algorithms are genuinely able to identify, match, and track) is always lower than the one transiting onto the water
surface and therefore, the extra seed practice is recommended. However, Wwe are aware that this recommendation may not
be practical in all conditions since fixed cameras can operate remotely without the necessity to be in-person at the field site,
and ~~Furthermore~~, deploying material in wide channels or difficult-to-access areas ~~can~~ may be challenging.

Following dimensional considerations, a model of the image-based errors can be formulated. Since the only variables
620 considered in this study were the ~~aggregation-spatial clustering~~ level and the seeding density, it is hypothesised that these errors
depend on only these variables. In functional form

$$f(\epsilon, \nu, \rho, \rho_{cv1}) = 0, \quad (3)$$

where f ~~=is a generic~~ function, and ρ and ρ_{cv1} are the seeding density and the ~~converging-reference~~ seeding density at $\nu = 1$
(Poisson case taken as a reference). According to the Buckingham- π theorem, Eq. (3) can be rewritten in terms of
dimensionless parameters as follows:

$$\epsilon = f\left(v, \frac{\rho}{\rho_{cv1}}\right). \quad (4)$$

625 The function f is usually considered as a multiplication of power laws (Buckingham, 1914; Evans, 1972; Melville and Sutherland, 1988; Pizarro et al., 2017b). In this study, we partially follow this approach and also hypothesise that the functional relationship f is described by a two-parameter exponential function:

$$\epsilon = c_1(1 - e^{-c_2 \#SDI}), \quad (5)$$

where $\#SDI = v^{k_1} \left(\frac{\rho}{\rho_{cv1}}\right)^{k_2}$ is the multiplication of power laws; and, c_1, c_2, k_1, k_2 are fitting coefficients. Model performance was quantified by means of the root mean square error (RMSE) and the Nash-Sutcliffe efficiency (NSE) for prediction of the image-velocimetry errors. In turn, the fitting coefficients were calibrated using the MATLAB genetic algorithm optimising RMSE. Table 1 summarises the results of the calibration process for both PTV and PIV, while Figure 5 shows the image-velocimetry errors ~~in~~ as a function of SDI, and observed versus computed errors. ~~It is observed from Eq. (5)~~ Figure 5 indicates that ~~and~~ SDI can correctly reproduced the main dynamics of the image-velocimetry errors, reporting low RMSE values in calibration (5.34 and 5.77% for PIV and PTV, respectively). A visual inspection of Figure 5.A1 and 5.B1 shows that increasing SDI values leads to higher errors for both image-velocimetry techniques. Figure 5.A2 and 5.B2 also show that the predictive capacity of Eq. (5) is higher at low PTV and PIV error values.

635 Even though PIV and PTV work differently, the fitted values in Eq. (5) were similar. Remarkably, k_1 and k_2 showed that the dimensionless SDI parameter can be approximated and used in practice as $\#SDI = v^{0.1} / \left(\frac{\rho}{\rho_{cv1}}\right)$. Furthermore, considering that the errors are minimised when SDI takes low values, SDI can be used in field conditions as a descriptor to choose the optimal portion of a video to analyse in order to minimise the errors in image-velocimetry estimates as a function of seeding density and aggregation-spatial clustering level. This novel idea is explored in the next subsection, taking the Basento River as a proof-of-concept case study.

645 **Table 1. Calibrated values of c_1, c_2, k_1, k_2 and model performances in terms of RMSE (%) and NSE. PTV and PIV calibration results. ρ_{cv1} values for PIV and PTV were taken from Figure 4 and are 1.52E-03 and 1.02E-03, respectively.**

	c_1	c_2	k_1	k_2	RMSE (%)	NSE
PTV	-71.87	0.04	0.10	-1.09	5.77	0.92
PIV	-78.49	0.07	0.10	-1.06	5.34	0.97

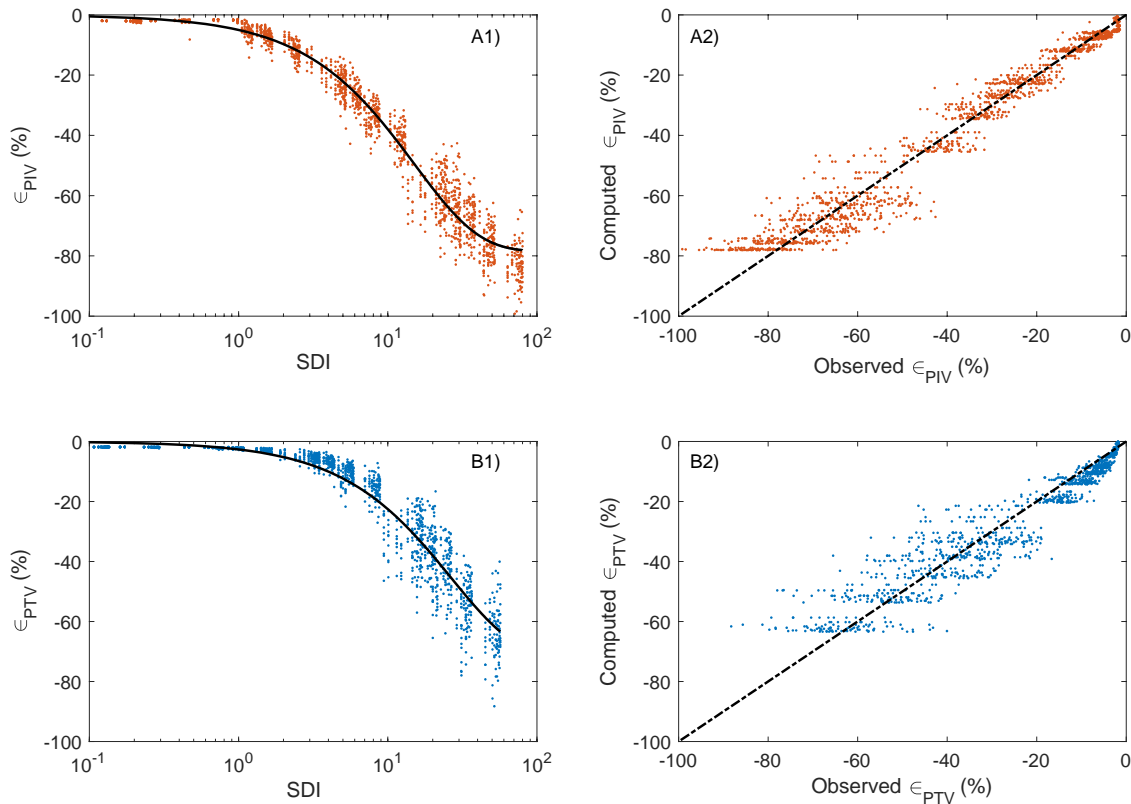


Figure 5. Image-velocimetry errors in function of **SDI** (A1 and B1) and observed versus computed errors (A2 and B2). Blue and orange colours are related to PTV and PIV numerical error results. Solid lines represent Eq. (5), while the dashed lines are the perfect agreement between observed and computed image-velocimetry errors.

3.2 Field Campaign: The Basento case study

Outcomes of the numerical analysis were tested on a real case study in order to identify the best temporal window (i.e., a subset of the video sequences) for image velocimetry analyses. The case study was selected due to the spatial distribution of tracers varying significantly during the recording period, making it challenging-subjective to manually select the optimal frames for analysis. Figure 6 displays a pre-processed frame with the location of the measuring points using standard field equipment (from L1 to L11). These surface flow velocity measurements were taken as reference velocities for PTV and PIV benchmarking. Figure 6.B and 6.C show a zoom of the ROI and the identification of transiting features, respectively. An example of identified features is presented in Figure 6.D. In this Figurefigure, the number of features, their relative positions and associated areas were identified using an ad-hoc algorithm recently-developed by Dal Sasso et al. (2020). the authors. This algorithm was recently introduced by Dal Sasso et al. (2020), detecting seeding characteristics for image-velocimetry purposes. Moving fFeatures – that can be blobs, regions of uniform intensity, or local corners – are detected and processed to derive This enables characterisation-of the seeding properties (i.e., empirical seeding densities and aggregation spatial clustering-levelsdistribution of tracers) on a frame-by-frame basis even if shapes and dimensions of the tracers vary

665 considerably. Using this approach, the empirical aggregation-spatial clustering level (i.e., the empirical one equivalent to that
 used in the numerical simulations), was quantified through the spatial dispersion index $D^* (= D/D_{Poisson} = \frac{\sigma^2 - \text{Var}(N)}{E(N)} + 1)$, where $\sigma^2 - \text{Var}(N)$ and $E(N)$ are the variance and mean values of the seeding density number of tracers N ,
 670 respectively, computed in sub-patches of the same size). This metric is normally a-measured to quantify whether a set of
 events are clustered or dispersed. Important to notice, D^* is assumed as an estimator of ν due to their similar properties such
as As in the numerical case, $D^* = \nu = 1$ which means features follow a Poisson distribution, while $D^* < 1$ ($\nu < 1$) and
 $D^* > 1$ ($\nu > 1$) follow an over- and under-dispersed spatial distribution, respectively.

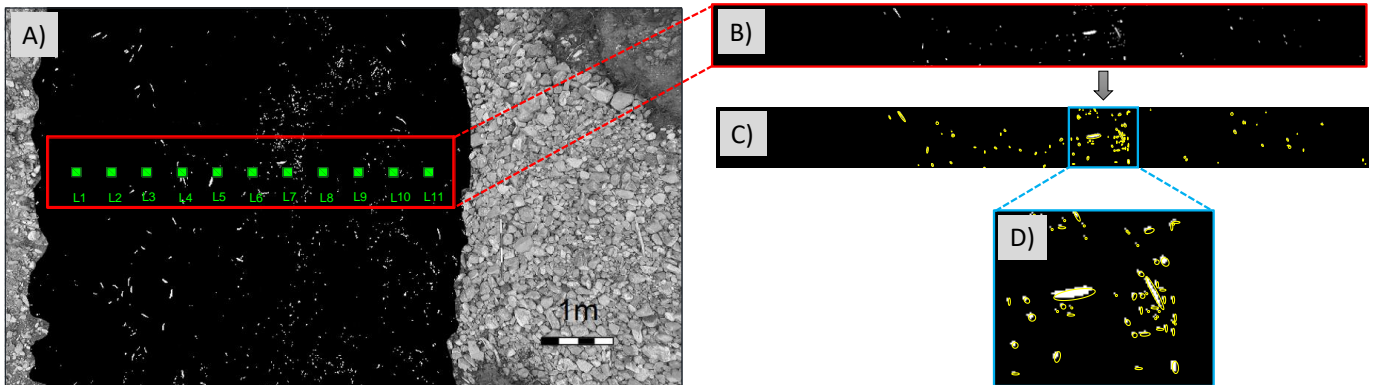


Figure 6. A) Pre-processed frame indicating the ROI and the reference measuring locations for benchmark purposes. The isolation of the ROI is presented in B), while in C) an example of identified features on the water surface. D) Zoom of an arbitrary portion of the ROI with the identified features.

675 Figure 7 shows a comprehensive overview of the seeding behaviour during the 200 frames considered for the analysis. Figure
 7.A and 7.B present the seeding density in ppp, and the dispersion index D^* computed as a function of the frame number. The
 minimum and maximum values for seeding density – and dispersion index – were $1.3E-04$ and $2.9E-03$ (ppp) – and 4.1 and
 57.3 –, respectively. Additionally, the estimated mean area of features (computed frame-by-frame and inside the ROI) varied
 between 1.5 and 3.5 cm^2 approximately.

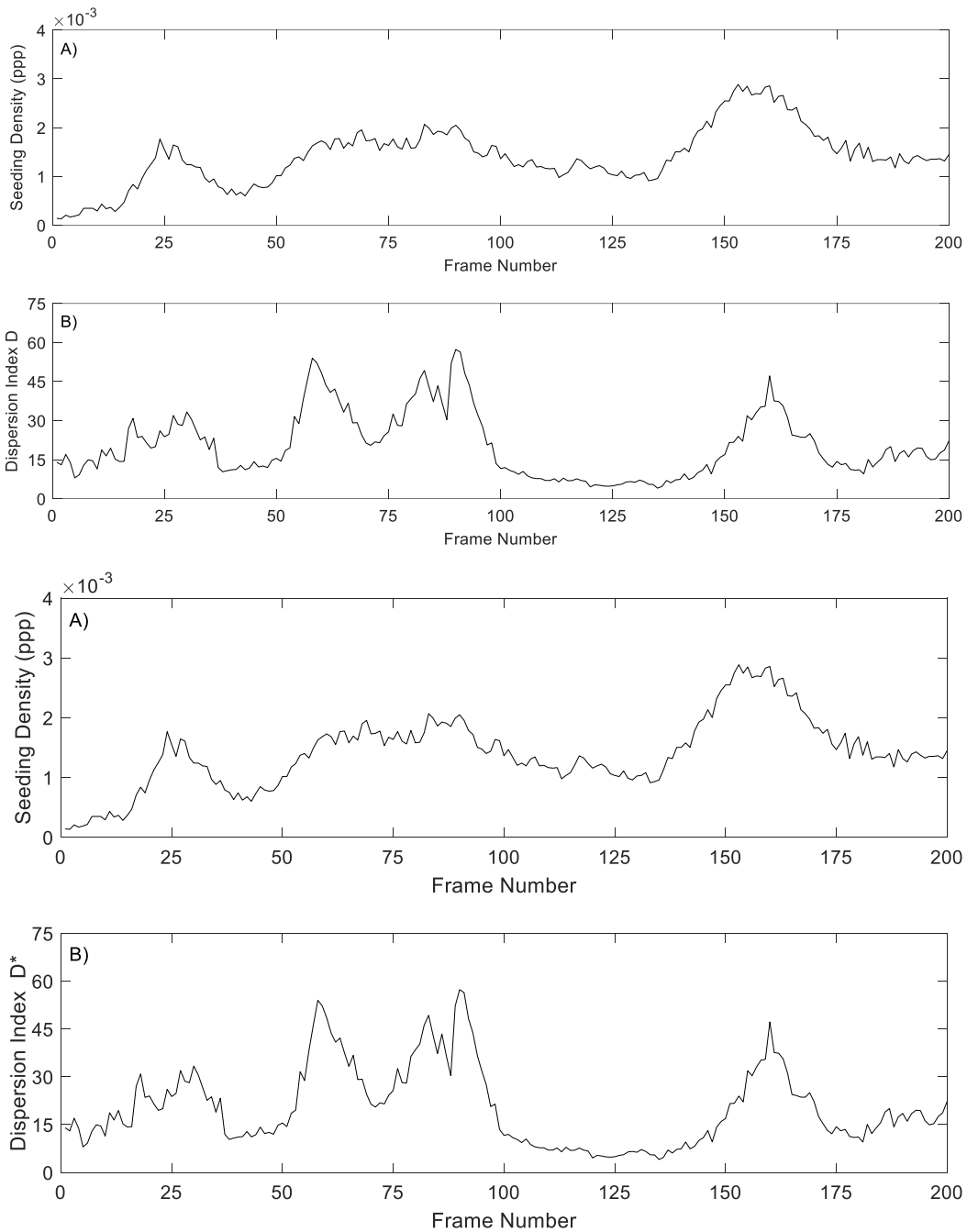


Figure 7. Overview of seeding characteristics on the ROI of the Basento River during the acquisition time: A) Seeding density in ppp, B) Dimensionless dispersion index D^* .

The approach mentioned above made it possible to compute $SDI \#$ and correctly identify the worst and best part of the video for image velocimetry analysis. A moving frame window length of 100 frames was arbitrarily chosen, on which an average

680

685

dispersion index D^2 and seeding density ~~was were~~ computed. This decision was motivated to increase the odds of populating the entire ROI with features. The empirical \overline{SDI} was then calculated as $\overline{SDI} = \overline{D}^{0.1} / \left(\frac{\overline{\rho}}{\rho_{cv1}} \right)$, where \overline{D} and $\overline{\rho}$ are the average-in-100-frames dispersion index and seeding density, respectively. Figure 8.A depicts \overline{SDI} in function of the frame windows. Triangle markers correspond with the minimum and maximum value of \overline{SDI} and their respective locations (82-181 and 1-100, respectively). Figure 8.A shows the particular case of PTV; nevertheless, PIV presented similar results. The locations of the minimum and maximum \overline{SDI} values was, therefore, unaffected by the image-velocimetry technique under consideration.

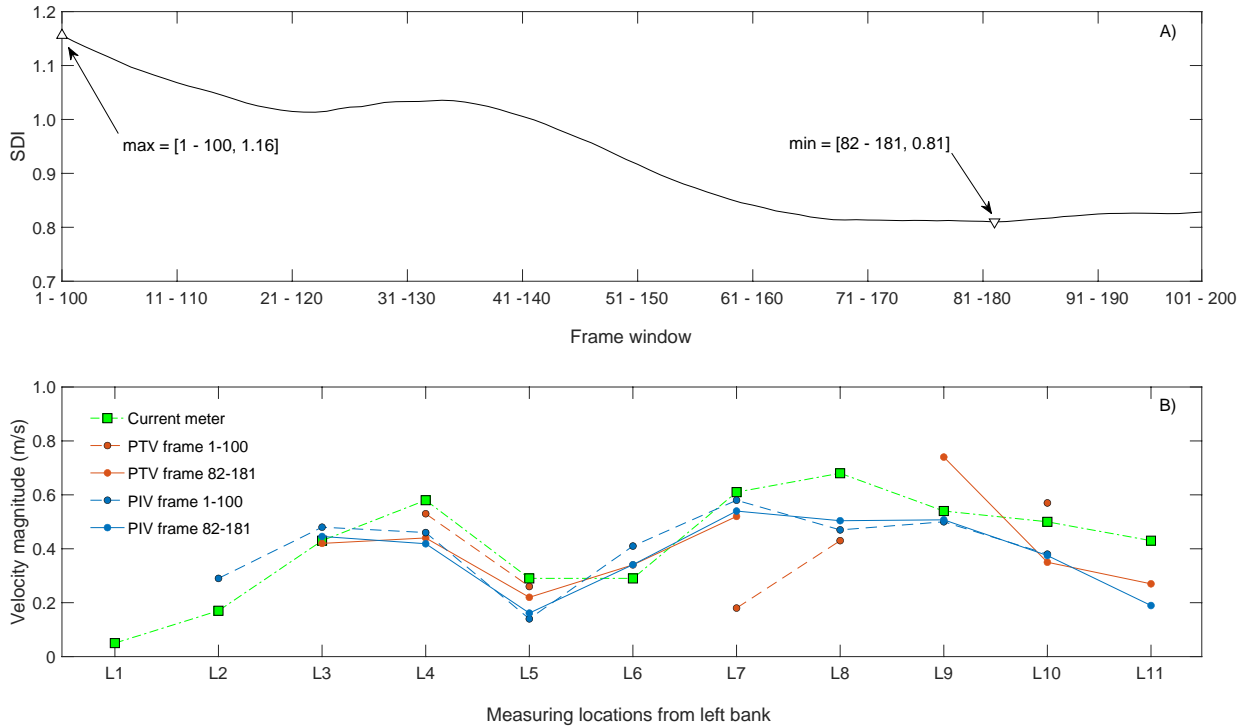


Figure 8. A) \overline{SDI} in function of the frame windows considering 100 frames. Triangle markers correspond with the minimum and maximum value of \overline{SDI} . Their locations were 82-181 and 1-100, respectively. Particular case of PTV, whereas PIV showed similar results and the locations of the minimum and maximum \overline{SDI} values were unaffected by the image-velocimetry technique. B) Comparison between PTV and PIV data for experiments on the Basento River. Values recorded with the current meter are also reported for a rapid visual assessment (green squares). Blue and orange colours represent PTV and PIV data.

Image-based velocity results were averaged in a block of $30 \times 30 \text{ cm}^2$ for a fair comparison among PTV, PIV, and benchmark velocity values. The measuring locations corresponded with the centre of the blocks. Computed velocities across the cross-section and reference velocities are reported in Figure 8.B. The blue and orange colours are associated with PTV and PIV results, respectively (same colours used within numerical results for consistency and fast visual comparison). Green squares are the velocities measured using the current meter. Notably, the measuring location L1 had no computed velocity values due to the lack of features transiting on this part of the ROI, whereas only PIV was able to compute velocities at L2. This issue can be explained due to the inherent property of PIV ~~that is able~~ to identify and track ~~other non-seeded~~ features such as ripples and

705 other structures transiting on the water surface. Interestingly, and in agreement with numerical results, 80% (frames 1-100) and 75% (frames 82-182) of the computed velocity measuring locations underestimated the reference velocities using PTV. Similarly, results using PIV were 67 and 78%, respectively. Therefore, a close agreement was observed with the numerical results that systematically presented underestimations of computed velocities in comparison with the ~~numerically theoretical imposed numerical~~ one. ~~The computed errors using PTV, PIV, and the total number of frames available were 23.93% and 23.69%, respectively. Interesting to mention is also the fact that~~ ~~Moreover, considering adopting~~ the optimal frame window ~~ensured that image-velocimetry measurements were produced for a greater or equal proportion of the channel than that produced by using frames allowed the computation of velocities over more reference locations than using frames~~ 1 - 100 (PTV: 72.7% vs 45.5% ~~of the channel width~~; PIV: 81.8% vs 81.8%).

715 Both image-velocimetry approaches correctly captured the mean behaviour of velocities across the cross-section. Table 2 presents summarised information of the average-in-100-frames seeding density and dispersion index as well as the initial and final frame used for image-velocimetry purposes. The \overline{SDI} π -value is also presented as well as the absolute average error across the cross-section. As expected from numerical analyses, an error reduction of about 15.9% (PTV) and 16.1% (PIV) was found on the Basento case study by employing the optimal frame window that minimises \overline{SDI} π . It is therefore recommended that \overline{SDI} π is used as a descriptor of the optimal portion of a video to analyse.

720

Table 2. Overview of features characteristics, minimum and maximum π values, and absolute errors using PTV and PIV. Values in parenthesis correspond with the error reduction using the optimal frame window.

Frames (from – to)	$\bar{\rho}$ (ppp)	\bar{D}	\overline{SDI} π		Absolute average Error (%)		Absolute Error Eq. (5) (%)	
			PTV	PIV	PTV	PIV	PTV	PIV
1 - 100	1.2E-03	26.1	1.16	1.72	27.72	28.74	3.70	8.91
82 - 181	1.7E-03	18.2	0.81	1.21	23.31 (15.9)	24.11 (16.1)	2.61 (29.5)	6.36 (28.6)

725 Finally, considering numerical findings, field image-based estimates presented larger errors in comparison with numerical results for the respective same values of \overline{SDI} π (last two columns of Table 2). This is despite the average seeding density being relatively high ($\sim 1.5E-03$) and the average dispersion index relatively low (~ 20). Possible reasons for deteriorations in PTV and PIV estimates can be attributed to other variables such as video stabilisation issues, noise due to different environmental conditions (e.g., intermittent and different levels of illumination, water reflections, and presence of shadows), and different shapes and dimensions of features (stressing the matching and tracking process between consecutive frames). ~~At In~~ this regard, ~~Dal Sasso et al. (2020) recently introduced some~~ metrics for the quantification of seeding characteristics needed to enhance image-velocimetry performances in rivers. Among them, the seeding density, ~~aggregation-spatial clustering~~ level, and coefficient of variation of tracers' dimension were statistically significant to velocity estimation accuracy. These issues should be the subject of further investigation, along with the application of these ideas to case studies with very different field conditions to assess the uncertainty of computed surface velocities and remote river flow estimates.

735 4 Strengths and limitations

735 One of the main strengths of this study ~~was~~ the introduction of the new dimensionless SDI index, which combines seeding characteristics – seeding density and spatial clustering of tracers – for image-velocimetry purposes. A numerical framework of synthetically generated images was adopted to isolate seeding effects on the performance of PIV and PTV performances analysis. This numerical framework allowed the generation of moving tracers with the possibility to vary the seeding density and spatial clustering of tracers. Additionally, one field case study was used to test and validate numerical findings. However, among the limitations, the numerical framework considered a constant and unidirectional imposed velocity only. Besides, PIV and PTV were set to run using a single configuration (e.g., PIV used FFT with a three-pass correlation method with fixed SA and IA rather than other combinations of SA and IA or an ensemble correlation method). The field case study was artificially seeded to enhance the identification and tracking of moving patterns on the water surface. Interestingly, 740 the dispersion index D^* was used as an empirical estimator of the numerical clustering level of tracers ν . D^* and ν share some interesting properties, which are useful to characterise under- and over-dispersed spatial distribution of tracers in practical applications. Finally, the errors computed using all frames available (frames 1 - 200) versus the optimal frame window (frames 82 - 181) were of the same order of magnitude, even though the number of frames used with SDI was the half of the total available. As a consequence, the quality of the seeding characteristics seemed to be more critical than the duration of the 745 footage. Of course, many other factors may affect the quality of the videos and consequently, the performance of image velocimetry estimates, but this assessment focuses specifically on the spatial distribution of tracers. In the field, other factors such as illumination conditions, shading on the scene, light reflections, presence of turbulent fluxes, vibration of the camera – among others – may further affect overall quality of the analysis, and these should be the subject of further assessment.

750 4.5 Conclusions

755 In this paper, we investigated the performances of PTV and PIV for surface flow velocity estimations. Synthetic generation of 33,600 images was ~~generated-performed~~ to test image-velocimetry techniques under different levels of seeding density and spatial-tracer aggregation and dispersion spatial clustering-seeding density. In all numerical cases, velocity results systematically underestimated the ~~theoretical~~ imposed numerical velocity. A general trend was observed by-in which increasing the seeding density and decreasing the level of ~~aggregation-tracers spatial clustering, in which results were~~ improved results. The main 760 advantage of the numerical ~~proposed~~ approach adopted is the controlled conditions in which the analyses can be conducted, minimising the effects of external disturbances. ~~This later helped to visualise the hidden trends that optimise image-based estimates.~~ Based on numerical findings, seeding densities lower than 1.0E-03 produced larger errors and ~~in~~ consequently, flows should be extra-seeded in field campaigns for optimal implementation of image velocimetry methods. Additionally, the dimensionless ~~SDI π parameter-index~~ was introduced as a descriptor of the optimal portion of the video to analyse using the 765 studied image-based techniques. Based on numerical results, SDI π can be approximated and used in practice as π SDI =

$\nu^{0.1} / \left(\frac{\rho}{\rho_{cv1}} \right)$, where ν , ρ , and ρ_{cv1} are the aggregation-spatial clustering level, the seeding density, and the converging seeding density at $\nu = 1$, respectively. A reduction of image-based errors was observed ~~by decreasing the~~ with lower values of SDI π . The Basento field case study (located in southern Italy) was considered as a proof-of-concept of the proposed framework. Seeding characteristics were empirically estimated through using a novel algorithm recently developed by the authors, opening
770 the possibilities of more refined analyses. The number of features, relative positions, and associated areas were saved for the computation of the empirical seeding densities and aggregation-spatial clustering levels. The empirical SDI π values were then computed, and two extreme cases were considered for velocimetry comparison purposes: i) the one considering the maximum value of SDI π (worst case), and ii) the one related to the minimum SDI π (best case). Field results corroborated numerical findings, and an error reduction of about 15.9 and 16.1% was achieved for PTV and PIV approaches respectively by using the
775 optimal frame window that minimises SDI for then calculated using PTV and PIV, respectively on the Basento case study by employing the optimal frame window. The optimal frame window was defined as the one that minimises SDI π . ~~Interest in~~ Interestingly to note, field image-based estimates presented larger errors than numerical results for the respective same values of SDI π . Possible reasons for deteriorating PTV and PIV estimates can be attributed to other variables such as: i) video stabilisation issues; ii) ~~intermittent and different~~ variable levels of illumination, water reflections, and presence of
780 shadows; and, iii) different shapes and dimensions of seeding features, stressing the importance of the feature matching and tracking process between consecutive frames. Further assessment is required to evaluate the significance of these factors in contributing to the uncertainty in image-velocimetry estimates across a range of hydrological and environmental conditions. The authors are keen to apply these ideas to further assess the uncertainty in remote flow velocities and river discharge estimates.

785 *Data availability:* Numerical and field data used in this study are available at Pizarro et al. (2020), <http://doi.org/10.5281/zenodo.3761859>.

Author contributions: AP conceptualised the study, wrote the scripts, processed and analysed the data, and drafted the paper. SD analysed the field data. SM coordinated the research activities and defined the research project. SD, MP, and SM contributed to the writing and reviewed the manuscript.

790 *Competing interests:* The authors declare no conflict of interest.

Acknowledgements: This work was funded by the COST Action CA16219 “HARMONIOUS—Harmonization of UAS techniques for agricultural and natural ecosystems monitoring”.

References

Adrian, R.: Particle-Imaging Techniques For Experimental Fluid-Mechanics, Annu. Rev. Fluid Mech.,

- 795 doi:10.1146/annurev.fluid.23.1.261, 1991.
- Adrian, R. J.: Twenty years of particle image velocimetry, *Exp. Fluids*, 39(2), 159–169, 2005.
- Anderson, K. E., Paul, A. J., McCauley, E., Jackson, L. J., Post, J. R. and Nisbet, R. M.: Instream flow needs in streams and rivers: The importance of understanding ecological dynamics, *Front. Ecol. Environ.*, doi:10.1890/1540-9295(2006)4[309:IFNISA]2.0.CO;2, 2006.
- 800 Batalla, R. J. and Vericat, D.: Hydrological and sediment transport dynamics of flushing flows: Implications for management in large Mediterranean rivers, *River Res. Appl.*, doi:10.1002/rra.1160, 2009.
- Bechle, A., Wu Chin, H., Liu, W.-C. and Kimura, N.: Development and Application of an Automated River-Estuary Discharge Imaging System, *J. Hydraul. Eng.*, 138(4), 327–339, doi:10.1061/(ASCE)HY.1943-7900.0000521, 2012.
- Brevis, W., Niño, Y. and Jirka, G. H.: Integrating cross-correlation and relaxation algorithms for particle tracking velocimetry, 805 *Exp. Fluids*, 50(1), 135–147, 2011.
- Buckingham, E.: On physically similar systems; Illustrations of the use of dimensional equations, *Phys. Rev.*, doi:10.1103/PhysRev.4.345, 1914.
- Cardwell, N. D., Vlachos, P. P. and Thole, K. A.: A multi-parametric particle-pairing algorithm for particle tracking in single and multiphase flows, *Meas. Sci. Technol.*, 22(10), 105406, 2011.
- 810 Le Coz, J., Hauet, A., Pierrefeu, G., Dramais, G. and Camenen, B.: Performance of image-based velocimetry (LSPIV) applied to flash-flood discharge measurements in Mediterranean rivers, *J. Hydrol.*, 394(1), 42–52, 2010.
- Dal Sasso, S. F., Pizarro, A., Samela, C., Mita, L. and Manfreda, S.: Exploring the optimal experimental setup for surface flow velocity measurements using PTV, *Environ. Monit. Assess.*, 190(8), doi:10.1007/s10661-018-6848-3, 2018.
- Dal Sasso, S. F., Pizarro, A. and Manfreda, S.: Metrics for the quantification of seeding characteristics to enhance image 815 velocimetry performance in rivers, *Remote Sens.*, doi:10.3390/rs12111789, 2020.
- Detert, M., Johnson, E. D. and Weitbrecht, V.: Proof-of-concept for low-cost and non-contact synoptic airborne river flow measurements, *Int. J. Remote Sens.*, doi:10.1080/01431161.2017.1294782, 2017.
- Efron, B.: Double exponential families and their use in generalized linear regression, *J. Am. Stat. Assoc.*, doi:10.1080/01621459.1986.10478327, 1986.
- 820 Eltner, A., Sardemann, H. and Grundmann, J.: Technical Note: Flow velocity and discharge measurement in rivers using terrestrial and unmanned-aerial-vehicle imagery, *Hydrol. Earth Syst. Sci.*, 24(3), 1429–1445, doi:10.5194/hess-24-1429-2020, 2020.
- Evans, J. H.: Dimensional Analysis and the Buckingham Pi Theorem, *Am. J. Phys.*, doi:10.1119/1.1987069, 1972.
- Fujita, I., Muste, M. and Kruger, A.: Large-scale particle image velocimetry for flow analysis in hydraulic engineering 825 applications, *J. Hydraul. Res.*, 36(3), 397–414, 1998.
- Good, S. P., Rodriguez-Iturbe, I. and Caylor, K. K.: Analytical expressions of variability in ecosystem structure and function obtained from threedimensional stochastic vegetation modelling, *Proc. R. Soc. A Math. Phys. Eng. Sci.*, doi:10.1098/rspa.2013.0003, 2013.

- Huang, W. C., Young, C. C. and Liu, W. C.: Application of an automated discharge imaging system and LSPIV during typhoon events in Taiwan, *Water (Switzerland)*, doi:10.3390/w10030280, 2018.
- 830 ISO, I. S. O.: 748, Measurement of Liquid Flow in Open Channel—Velocity-Area Methods. 1997, 1997.
- Leitão, J. P., Peña-Haro, S., Lüthi, B., Scheidegger, A. and Moy de Vitry, M.: Urban overland runoff velocity measurement with consumer-grade surveillance cameras and surface structure image velocimetry, *J. Hydrol.*, doi:10.1016/j.jhydrol.2018.09.001, 2018.
- 835 Lloyd, P. M., Stansby, P. K. and Ball, D. J.: Unsteady surface-velocity field measurement using particle tracking velocimetry, *J. Hydraul. Res.*, 33(4), 519–534, 1995.
- Manfreda, S.: On the derivation of flow rating curves in data-scarce environments, *J. Hydrol.*, doi:10.1016/j.jhydrol.2018.04.058, 2018.
- Manfreda, S., Caylor, K. K. and Good, S. P.: An ecohydrological framework to explain shifts in vegetation organization across climatological gradients, *Ecohydrology*, doi:10.1002/eco.1809, 2017.
- 840 Manfreda, S., Link, O. and Pizarro, A.: A theoretically derived probability distribution of scour, *Water (Switzerland)*, doi:10.3390/w10111520, 2018a.
- Manfreda, S., McCabe, M. F., Miller, P. E., Lucas, R., Madrigal, V. P., Mallinis, G., Dor, E. Ben, Helman, D., Estes, L., Ciruolo, G., Müllerová, J., Tauro, F., de Lima, M. I., de Lima, J. L. M. P., Maltese, A., Frances, F., Caylor, K., Kohv, M., Perks, M., Ruiz-Pérez, G., Su, Z., Vico, G. and Toth, B.: On the use of unmanned aerial systems for environmental monitoring, *Remote Sens.*, doi:10.3390/rs10040641, 2018b.
- 845 Manfreda, S., Pizarro, A., Moramarco, T., Cimorelli, L., Pianese, D. and Barbetta, S.: Potential advantages of flow-area rating curves compared to classic stage-discharge-relations, *J. Hydrol.*, 124752, 2020.
- Melville, B. W. and Sutherland, A. J.: Design method for local scour at bridge piers, *J. Hydraul. Eng.*, 114(10), 1210–1226, 1988.
- 850 Muste, M., Fujita, I. and Hauet, A.: Large-scale particle image velocimetry for measurements in riverine environments, *Water Resour. Res.*, 44(4), 2008.
- Nobach, H., Damaschke, N. and Tropea, C.: High-precision sub-pixel interpolation in particle image velocimetry image processing, *Exp. Fluids*, 39(2), 299–304, 2005.
- 855 Ohmi, K. and Li, H.-Y.: Particle-tracking velocimetry with new algorithms, *Meas. Sci. Technol.*, 11(6), 603, 2000.
- Owe, M.: Long-term streamflow observations in relation to basin development, *J. Hydrol.*, 78(3–4), 243–260, 1985.
- Pearce, S., Ljubičić, R., Peña-Haro, S., Perks, M., Tauro, F., Pizarro, A., Dal Sasso, S., Strelnikova, D., Grimaldi, S., Maddock, I., Paulus, G., Plavšić, J., Prodanović, D. and Manfreda, S.: An Evaluation of Image Velocimetry Techniques under Low Flow Conditions and High Seeding Densities Using Unmanned Aerial Systems, *Remote Sens.*, doi:10.3390/rs12020232, 2020.
- 860 Perks, M., Sasso, S. F. D., Hauet, A., Coz, J. Le, Pearce, S., Peña-Haro, S., Tauro, F., Grimaldi, S., Hortobágyi, B., Jodeau, M., Maddock, I., Pénard, L. and Manfreda, S.: Towards harmonization of image velocimetry techniques for river surface

- velocity observations, *Earth Syst. Sci. Data Discuss.*, doi:10.5194/essd-2019-133, 2019.
- Perks, M. T., Russell, A. J. and Large, A. R. G.: Technical note: Advances in flash flood monitoring using unmanned aerial vehicles (UAVs), *Hydrol. Earth Syst. Sci.*, doi:10.5194/hess-20-4005-2016, 2016.
- Peterson, S. D., Chuang, H. S. and Wereley, S. T.: Three-dimensional particle tracking using micro-particle image velocimetry hardware, *Meas. Sci. Technol.*, doi:10.1088/0957-0233/19/11/115406, 2008.
- Pizarro, A., Samela, C., Fiorentino, M., Link, O. and Manfreda, S.: BRISENT: An Entropy-Based Model for Bridge-Pier Scour Estimation under Complex Hydraulic Scenarios, *Water*, doi:10.3390/w9110889, 2017a.
- 870 Pizarro, A., Ettmer, B., Manfreda, S., Rojas, A. and Link, O.: Dimensionless effective flow work for estimation of pier scour caused by flood waves, *J. Hydraul. Eng.*, 143(7), doi:10.1061/(ASCE)HY.1943-7900.0001295, 2017b.
- Pizarro, A., Silvano Fortunato, D. S., Perks, M. T. and Manfreda, S.: Data on spatial distribution of tracers for optical sensing of stream surface flow (Version 0.1), [Dataset] Zenodo, doi:10.5281/zenodo.3761859, 2020.
- Raffel, M., Willert, C. E., Scarano, F., Kähler, C. J., Wereley, S. T. and Kompenhans, J.: Particle image velocimetry: a practical guide, Springer., 2018.
- 875 Strelnikova, D., Paulus, G., Käfer, S., Anders, K.-H., Mayr, P., Mader, H., Scherling, U. and Schneeberger, R.: Drone-Based Optical Measurements of Heterogeneous Surface Velocity Fields around Fish Passages at Hydropower Dams, *Remote Sens.*, doi:10.3390/rs12030384, 2020.
- Tauro, F. and Grimaldi, S.: Ice dices for monitoring stream surface velocity, *J. Hydro-environment Res.*, 14, 143–149, 2017.
- 880 Tauro, F. and Salvatori, S.: Surface flows from images: ten days of observations from the Tiber River gauge-cam station, *Hydrol. Res.*, 48(3), 646–655, 2017.
- Tauro, F., Porfiri, M. and Grimaldi, S.: Orienting the camera and firing lasers to enhance large scale particle image velocimetry for streamflow monitoring, *Water Resour. Res.*, 50(9), 7470–7483, 2014.
- Tauro, F., Pagano, C., Phamduy, P., Grimaldi, S. and Porfiri, M.: Large-scale particle image velocimetry from an unmanned aerial vehicle, *IEEE/ASME Trans. Mechatronics*, 20(6), 3269–3275, 2015.
- 885 Tauro, F., Petroselli, A., Porfiri, M., Giandomenico, L., Bernardi, G., Mele, F., Spina, D. and Grimaldi, S.: A novel permanent gauge-cam station for surface-flow observations on the Tiber River, *Geosci. Instrumentation, Methods Data Syst.*, 5(1), 241–251, 2016.
- Tauro, F., Piscopia, R. and Grimaldi, S.: Streamflow Observations From Cameras: Large-Scale Particle Image Velocimetry or Particle Tracking Velocimetry?, *Water Resour. Res.*, 53(12), 10374–10394, 2017.
- 890 Tauro, F., Selker, J., Van De Giesen, N., Abrate, T., Uijlenhoet, R., Porfiri, M., Manfreda, S., Caylor, K., Moramarco, T., Benveniste, J., Ciraolo, G., Estes, L., Domeneghetti, A., Perks, M. T., Corbari, C., Rabiei, E., Ravazzani, G., Bogena, H., Harfouche, A., Broccai, L., Maltese, A., Wickert, A., Tarpanelli, A., Good, S., Lopez Alcala, J. M., Petroselli, A., Cudennec, C., Blume, T., Hut, R. and Grimaldia, S.: Measurements and observations in the XXI century (MOXXI): Innovation and multi-disciplinarity to sense the hydrological cycle, *Hydrol. Sci. J.*, doi:10.1080/02626667.2017.1420191, 2018.
- 895

- Tauro, F., Piscopia, R. and Grimaldi, S.: PTV-Stream: A simplified particle tracking velocimetry framework for stream surface flow monitoring, *Catena*, doi:10.1016/j.catena.2018.09.009, 2019.
- Thielicke, W. and Stamhuis, E. J.: PIVlab – Towards User-friendly, Affordable and Accurate Digital Particle Image Velocimetry in MATLAB, *J. Open Res. Softw.*, doi:10.5334/jors.bl, 2014.
- 900
- Wu, Q. X. and Pairman, D.: A relaxation labeling technique for computing sea surface velocities from sea surface temperature, *IEEE Trans. Geosci. Remote Sens.*, 33(1), 216–220, 1995.